PROBLEMY MECHATRONIKI
UZBROJENIE, LOTNICTWO, INŻYNIERIA BEZPIECZEŃSTWA

ISSN 2081-5891

9, 4 (34), 2018, 85-100

PROBLEMS OF MECHATRONICS
ARMAMENT, AVIATION, SAFETY ENGINEERING

Strength Analysis of a Ducted Axial Fan Blade

Marek ROŚKOWICZ, Ryszard CHACHURSKI, Sławomir TKACZUK, Piotr LESZCZYŃSKI*, Maciej MAJCHER, Łukasz OMEN

Military University of Technology, Faculty of Mechatronics and Aerospace,
2 gen. Witolda Urbanowicza Str., 00-908 Warsaw, Poland
Corresponding author's e-mail address: piotr.leszczynski@wat.edu.pl

Received by the editorial staff on 10 November 2017
The reviewed and verified version was received on 17 December 2018

DOI 10.5604/01.3001.0012.7334

Abstract. This paper presents a numerical strength analysis of a ducted axial fan blade. Ducted axial fans are a large group of fluid-flow machines. The analysis was designed to determine the causes of cyclic failures of a ventilation unit. The paper presents a reverse engineering approach to the mapping of the fan blade's geometrical features. The geometrical features were mapped by triangulation from the scanning images produced by a 3D optical scanner. These were followed by simplifying assumptions on which the numerical calculations were based. The numerical calculations were carried out at the operating rotational speeds of the ducted axial fan's rotor. The course of the numerical calculations is described, and their results are also presented herein. The results are represented on colour maps of stress distribution for selected structural elements of the fan blade. The stress distribution at a blade cross-section was compared to CT scans of the fractures of failed rotor blade airfoils. Final conclusions were developed which show that the design engineering process of fans should feature optimisation of the fan's efficiency, including the strength and performance parameters, which should include the service life of the fan.
Keywords: axial fan, reverse engineering, numerical calculations, strength calculations

1. BACKGROUND

Axial fans, and ducted axial fans specifically, are examples of fluid-flow machines intended for transferring working media from indoor rooms to the outdoor environment or in the reverse direction. Irrespective of their specific engineering solutions, fans are a very large group of fluid-flow machines currently applied in engineering, as evidenced by the data about the energy requirements of fan drive systems. In 2011, the overall electrical energy consumption of fans driven by electric motors within the power input range of 125 W to 500 kW was 344 TWh in the European Union alone; current forecast data suggest that if the current EU trends do not change, this electrical energy consumption level will increase to 560 TWh [9].

The EU and global-tier trends towards electrical energy efficiency, the reduction of CO_2 emissions and the reduction of mechanical equipment noise necessitate fan design with increasingly improved performance and efficiency. One of the approaches applied to improve the efficiency of fans is to modify their aerodynamic (fluid flow) systems [8, 10]. The primary focus of these modifications is the shape of the rotor blades [2]. Moreover, blade tips have been featuring winglets to reduce induced drag [1, 3] with grooving fabricated on the outer blade tip surfaces to improve the volumetric capacity of the fans [13]. The design of the fan rotor and its installation conditions are also important to the stability of the fan's performance [12, 16].

The design modifications aimed to improve the aerodynamic parameters of fans have resulted in highly twisted fan blades [2], which are now usually forward-swept or back-swept at a high angle [14], and/or with weight concentrations at the blade tips in the form of winglets. The design engineering applications intended to improve the efficiency of fans may directly contribute to the strength and performance characteristics of fan blades, which include fatigue strength.

This paper is an analysis of a failure case of a ducted axial fan which supplied cooling air for an electric generator set.

The ducted axial fan featured a maximum air flow rate of 92.6 m^3/h and a six-blade rotor, 1.265 m in diameter (Fig. 1), the maximum rotational speed of which was 1465 rpm. A very frequent in-service failure of this specific fan type was a rotor blade breaking off (Fig. 2); it was prudent then to run a strength analysis of the fan blades.

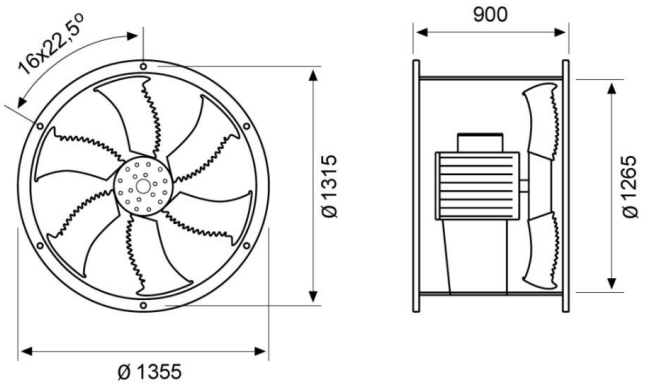

Fig. 1. Diagram of the ducted axial fan under analysis [15]

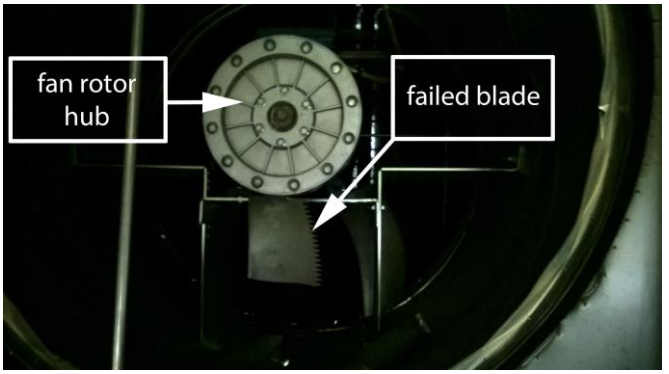

Fig. 2. Ducted axial fan rotor with broken off blades

2. MAPPING OF THE FAN GEOMETRICAL FEATURES

A virtual model of the ducted axial fan blade was developed to facilitate its numerical strength analysis. The blade was modelled from scanning images of a part of the rotor ring. The scanning images were captured with a GOM Atos 2 optical scanner in triangulation mode. Both optical scanner cameras were applied with scanning markers in the form of stripes applied adhesively to the blade. Each pixel of the image captured by the cameras was pre-analysed by calculation of the coordinates of the numerically analysed points. A cloud of points was the result of the pre-analysis.

The pre-mapped geometrical features of the blade included many discontinuities, including voids, broken curves, surfaces and edges, and surfaces which failed the continuity criteria applied. This was typical for physical objects scanned with this method. A body modelling software application was used to correct for the scanning deficiencies in the geometrical features of the blade.

To achieve the corrections, specific cross-sections along the blade span were modified to remove all spline discontinuities. The final stage of the work to improve the quality of the blade geometrical features was to define the surfaces of the mapped blade cross-sections.

The process of reproducing the blade's geometrical features finished with the serration on the blade's trailing edge and the reconstructed the blade tip winglet. The finished model of the blade is shown in Fig. 3.

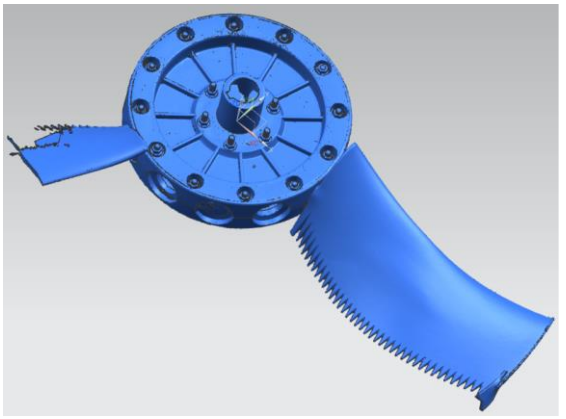

Fig. 3. Fully mapped geometry of a single fan blade with its hub

The degree of blade reproduction was visually assessed by superimposing the blade scan image on the reproduced blade model. Fig. 4 shows the visualised reproduction of the blade's shape.

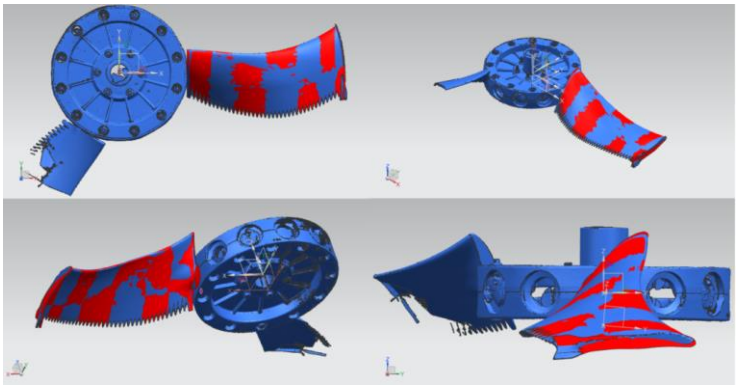

Fig. 4. Visualisation of the degree of reproduction (mapping) of the blade's geometrical features

With both sets of geometrical features interpenetrated, the authors assumed that the degree of blade reproduction was satisfactory. The produced blade geometry was input to the strength analysis.

3. STRENGTH ANALYSIS OF THE BLADE

The manufacturer of this ducted axial fan installed blades with curved attack edges and serrated trailing edges to optimise the aerodynamic performance and reduce the operating noise level (see Fig. 3). The blade airfoil featured a strong twist and a strong sweep; the mass centres of the blade cross-sections were aligned with the geometrical centreline of the blade and, due to the effect of centrifugal forces, resulted in additional bending and torsional moments applied to the blade airfoil (causing the blade to straighten and 'untwist' itself) [4]. The distribution of the blade cross-sectional surface areas along the blade radius was different than in aircraft turbine engines [11], in which the surface areas become smaller away from the blade locking piece towards the blade tip, which is beneficial to the stress distribution [5].

The strength analysis was completed by numerical calculations processed with the following simplifying assumptions:

- aerodynamic loads were omitted, as it was difficult to estimate them for the blade given the high turbulence found during fluid flow measurements;
- loads from aeromechanical vibrations were omitted (the air flow vibration in the flow passage and the mechanical vibrations);
- structural imperfections of the blade material, caused by the blade casting process, were omitted;
- the serrated blade trailing edge was replaced with a straight blade trailing edge;
- uniform strength parameters of the casting material of the blade (an aluminium alloy) were assumed.

The following blade airfoil material specifications were assumed: density $\rho = 2730$ kg/m^3, Young's E modulus = 69e3 MPa, Poisson's ratio $\nu = 0.33$.

The calculations were run for the blade airfoil, since an analysis of the witnessed blade failures had not suggested any strength insufficiency in the area of the blade locking pieces; the blade locking piece was modelled only to the extent required for applying the boundary conditions which represented the retention of the blade by its hub, i.e. to prevent displacement of the blade along the radius and the axis of rotation around the locking piece's axis.

The blade airfoil simplified in this way and subjected to the strength analysis is shown in Fig. 5.

The strength analysis was completed with a FEM (Finite Element Method) based software application for numerical calculations, Comsol Multiphysics v. 3.5a. The numerical calculations were run at the operating rotational speed range of 600÷1430 rpm.

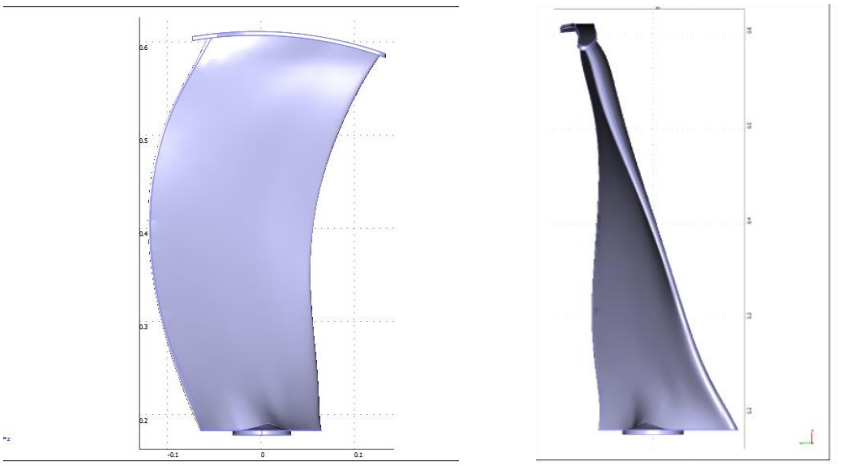

Fig. 5. Fan blade (the simplified computational model)

The von Mises reduced stress distribution in the superficial zone of the blade airfoil concave side is presented for an increasing rotational speed of the rotor in Figs. 6 to 10. It was important that although the stresses near the blade locking piece and the blade winglet were relatively low, as the rotor rotational speed increased, the stress values definitely increased in the superficial zone of the blade airfoil mid section, and especially near the blade trailing edge on the airfoil concave side, as shown in Figs. 11 to 13.

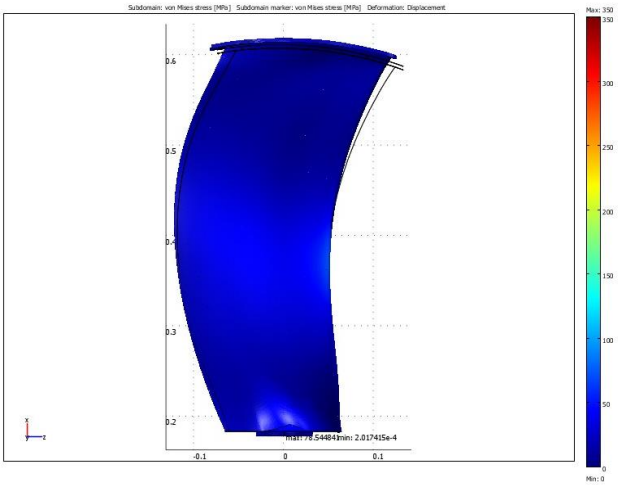

Fig. 6. Stress distribution within the surface zone of the blade airfoil at a rotor speed of 600 rpm

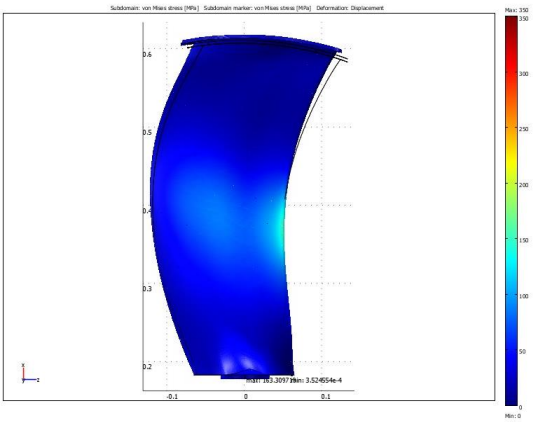

Fig. 7. Stress distribution within the surface zone of the blade airfoil at a rotor speed of 893 rpm

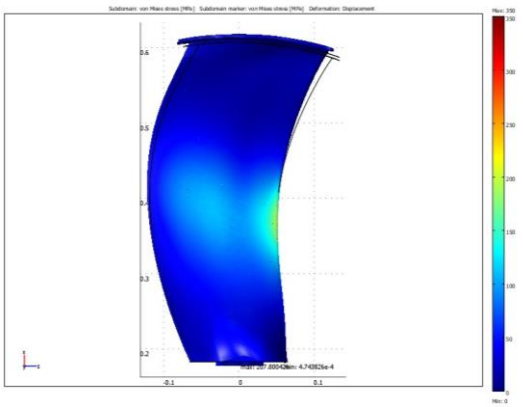

Fig. 8. Stress distribution within the surface zone of the blade airfoil at a rotor speed of 1025 rpm

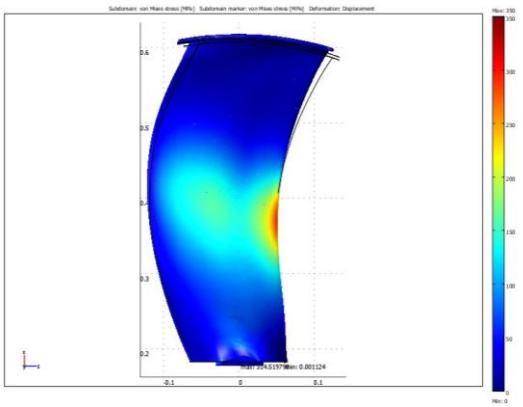

Fig. 9. Stress distribution within the surface zone of the blade airfoil at a rotor speed of 1318 rpm

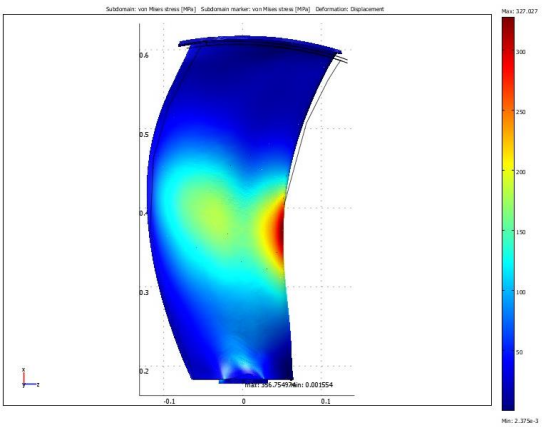

Fig. 10. Stress distribution within the surface zone of the blade airfoil (concave side) at a rotor speed of 1430 rpm

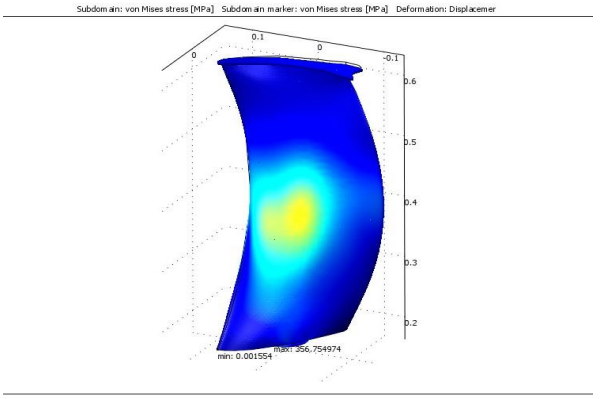

Fig. 11. Stress distribution within the surface zone of the blade airfoil (convex side) at a rotor speed of 1430 rpm

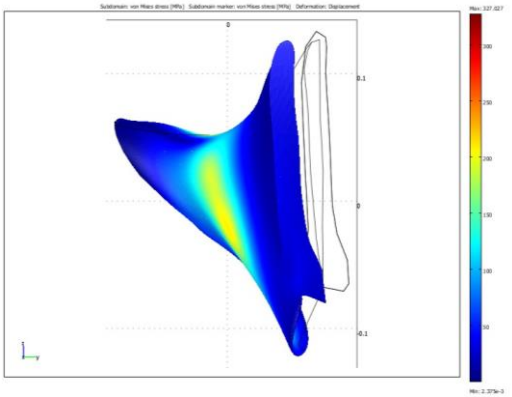

Fig. 12. Stress distribution within the surface zone of the blade airfoil (shown from the winglet side) at a rotor speed of 1430 rpm

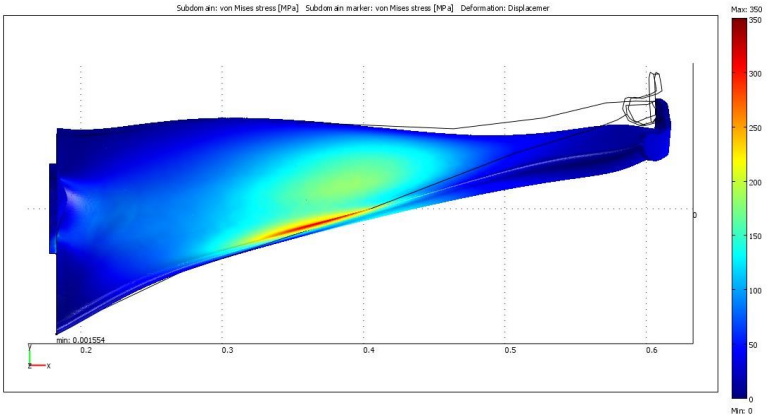

Fig. 13. Stress distribution within the surface zone of the blade airfoil (shown from the attack edge side) at a rotor speed of 1430 rpm

The analysis of the stress distributions at selected blade airfoil cross-sections confirmed that the stress values were low at the cross-section near the blade locking piece and the winglet, while reaching their maximums in the blade mid cross-sections (Figs. 14 to 15).

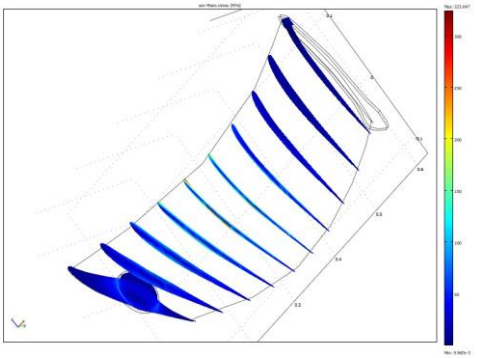

Fig. 14. Stress distribution within the blade airfoil cross-sections at a rotor speed of 1430 rpm

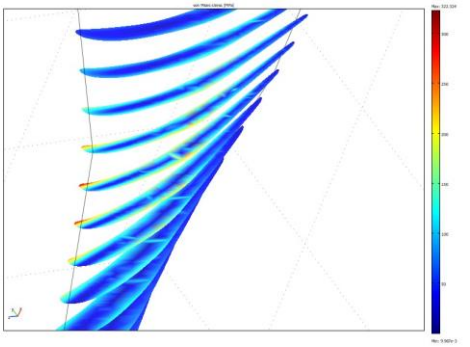

Fig. 15. Stress distribution within the blade airfoil mid cross-sections at a rotor speed of 1430 rpm

Figure 16 shows the stress distribution within the cross-section in the blade airfoil middle, which was 38.5 cm from the rotor's axis of rotation. The maximum stress values near the blade attack edge on the airfoil concave side and high stress values in the superficial zones in the middle of the airfoil chord (both on the concave and convex sides) were evident. The stress values in the middle of the blade airfoil were low along the entire airfoil chord. This stress distribution suggested that the blade airfoil torsional moments were a major contributor to the blade load.

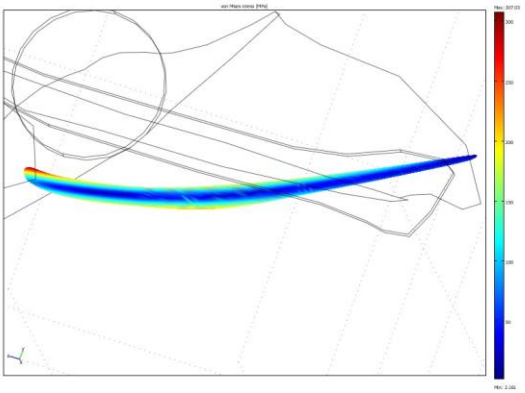

Fig. 16. Stress distribution within the blade airfoil mid cross-sections (at 38.5 cm from the rotor's axis of rotation) at a rotor speed of 1430 rpm

A comparison of the stress distribution within the blade cross-section shown in Fig. 16 to the photographic images of the fracture of the failed blades (Fig. 17) revealed that the origin points of fatigue fracture were located near the blade attack edge on the airfoil concave side. Evidence of fatigue failure was also identified in the superficial zones on the airfoil concave and convex side of some blades.

Most of the blades which suffered failure were broken in the middle of their length, where the numerical calculations revealed the maximum stress values to be.

Based on the numerical calculations, the authors estimated that the localised stress values could reach as high as 350 MPa, which was beyond the instantaneous strength of the blade material. The completed strength analysis led to a hypothesis that the failure of each rotor originated from fatigue failure of one of the blades. The fatigue failure was initiated in the mid section of the blade airfoil, where the stress values were at their maximum. The blade fragments detached by the failure collided and made other rotor blades fail by cracking in the middle or breaking off at the blade locking pieces (see Fig. 2).

The failure of the blades was not prevented by a modification made by the manufacturer, comprising steel bracing bars with auxiliary bars used in some design versions of the blades.

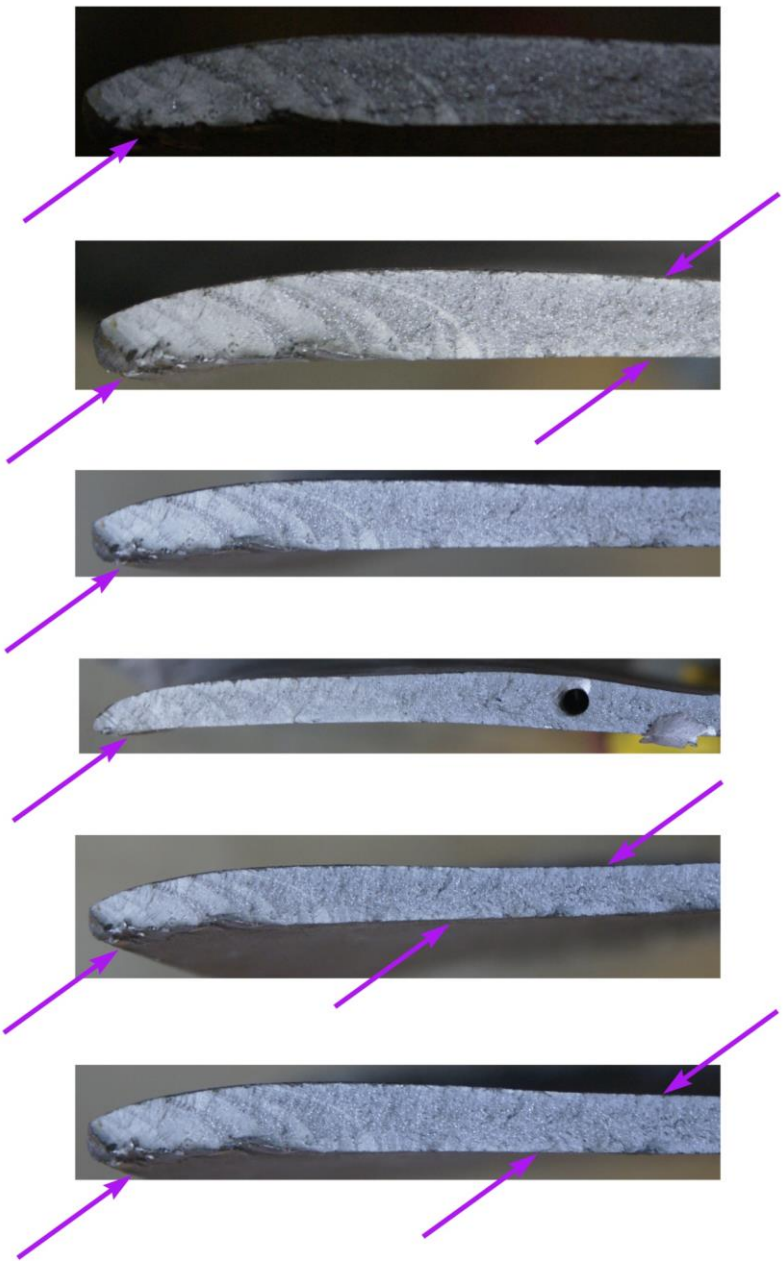

Fig. 17. Fractures shown of the failed rotor blades

The auxiliary bars were located at the most strained cross-sections of the blade; their presence contributed further to the weakening of this critical cross-section of the blade airfoil (Figs. 18 to 19).

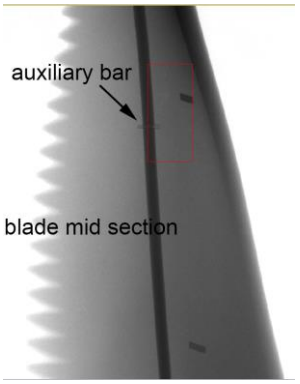

Fig. 18. CT scanned image of a blade's mid section, version with a bracing bar shown

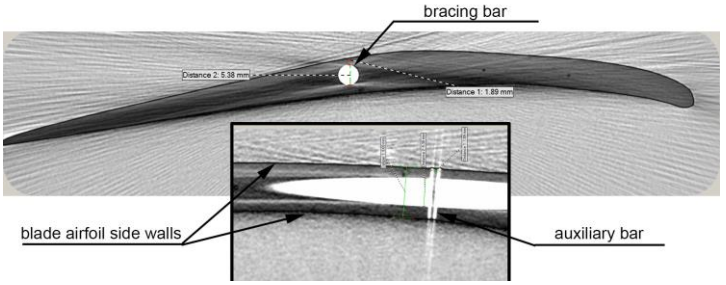

Fig. 19. Location of the auxiliary bar within its cross-section; view of the auxiliary bar installation between the two side walls of the blade airfoil (shown on a CT scan)

Figures 20 do 23 show examples of the numerical calculations run for a blade with a bracing bar and an auxiliary bar at a rotor speed of 1465 rpm.

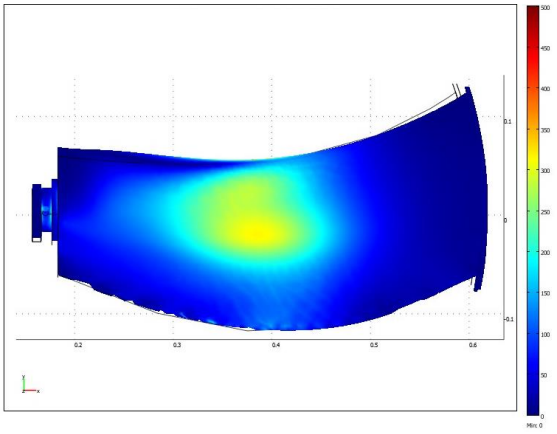

Fig. 20. Stress distribution within the surface zone of the blade airfoil (convex side) with the bracing bar at a rotor speed of 1465 rpm

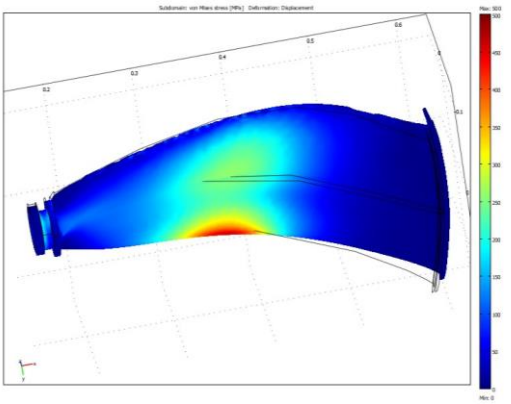

Fig. 21. Stress distribution within the surface zone of the blade airfoil (concave side) with the bracing bar at a rotor speed of 1465 rpm

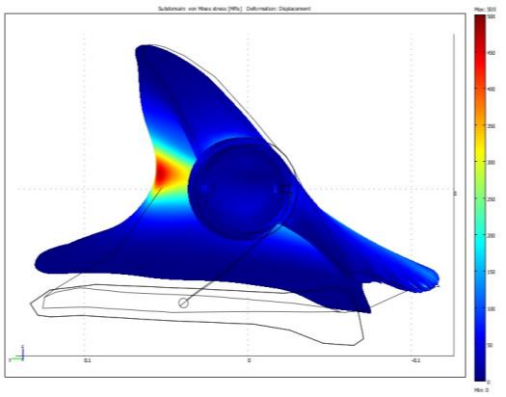

Fig. 22. Stress distribution within the surface zone of the blade airfoil (shown from the blade locking piece side) with the bracing bar at a rotor speed of 1465 rpm

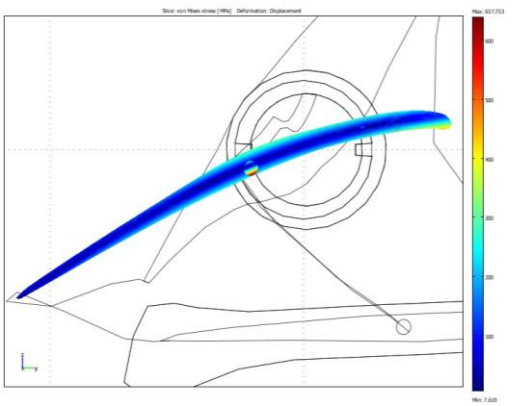

Fig. 23. Stress distribution within the blade airfoil mid cross-sections (at 38.3 cm from the rotor's axis of rotation) with the bracing bar at a rotor speed of 1465 rpm

The obtained results allowed for a conclusion that the modifications proposed by the manufacturer in the form of bracing bars did not reduce the stress levels at the critical blade cross-sections and failed to eliminate the reduced fatigue life of the blades.

4. CONCLUSION

The results of the numerical calculations and analyses allowed for the formulation of the following conclusions:

1. It seems that the blades under this investigation were optimised by their manufacturer only in terms of aerodynamic performance and maximum noise levels. Unfortunately, this optimisation failed to include significant problems with the strength and performance of the fan blades, including the very limited fatigue life.
2. The blade airfoil in its post-optimisation state is heavily twisted and swept; this, combined with an unusual distribution of the blade mass resulted in additional loads from torsional and bending moments, which cause localised concentrations of stress at the critical cross-section at the middle of the blade airfoil.
3. The most likely cause of the blade failures is a process of fatigue evolving in the blade material, initiated in the critical cross-section of the blade (the calculations narrow down the location of failure origin to the attack edge on the blade airfoil concave side, or the concave and convex sides near the surface of the blade airfoil).
4. The process of initiation and evolution of fatigue cracks was amplified further by the bracing pieces introduced to the blade design and comprising the bracing bar and the auxiliary bar which were crossing one another in the middle of the blade height with a poor adhesion to the blade material, instead of improving the mechanical performance of the blade. The bars significantly reduced the critical cross-section surface area, weakening the already strained blade structure and concentrating the stress.
5. This strength analysis omitted other factors unfavourable to the fatigue strength of the blades, such as variations in the rotor speed from the variable demand for cooling air, or operating restrictions of the inverter drives, and high-amplitude vibrations of aeromechanical origin. These omitted factors enhanced the negative effects of the initiation and propagation of in-service failure cracks in the blades of ducted axial fans.

This paper includes results of a commercial research work, ref. PBU 01-318, funded in the year 2015

REFERENCES

[1] Aerovent. Surge, Stall, and Instabilities in Fans. Information and Recommendations for the Engineer, Fan Engineering (FE – 600), Twin City Fan Companies Ltd., 2012.

[2] Bamberger Konrad, Thomas Carolus. 2012. *Optimization of axial fans with highly swept blades with respect to losses and noise reduction*. FAN 2012 Senlis (France), 18-20 April, 2012.

[3] Beskales Samer Anwer, Samir Sobhy Ayad, Maher Gamil Higazy, Osama Ezzet Abdellatif. 2013. The effect of tip end-blade geometry on the axial fans performance. In *Proceedings of Eleventh International Conference of Fluid Dynamics ICFD11*, Alexandria, Egypt, December 19-21, 2013.

[4] Dzierżanowski Paweł, Michał Łagosz, Ryszard Prociak. 1984. *Konstrukcja silników lotniczych. Wstęp. Część I. Konstrukcja silników turbinowych*. Warszawa: Wydawnictwo WAT.

[5] Dżygadło Zbigniew, Mieczysław Łyżwiński, Jerzy Otyś, Stefan Szczeciński, Ryszard. Wiatrek. 1982. *Napędy lotnicze. Zespoły wirnikowe*. Warszawa: Wydawnictwo WKiŁ.

[6] Fortuna Stanisław. 1999. *Wentylatory. Podstawy teoretyczne, zagadnienia konstrukcyjno-eksploatacyjne i zastosowanie*. Kraków: Wydawnictwo Techwent.

[7] Hendiger Jacek. 2012. „Akustyka instalacji wentylacyjnej, czyli: co szumi, co tłumi?". *Instal Reporter* 4.

[8] Álvarez Roberto Arias, Javier Fernando López. 2007."Fan protection against stalling phenomenon". *EUROVENT* 1/11.

[9] Regulation (EC) No. 327/2011 of 30 March 2011.

[10] SaskPower. Fans & Blowers. Energy Efficiency Reference Guide. CEATI International Inc., 2008.

[11] Szczeciński Stefan, Włodzimierz Balicki, Ryszard Chachurski, Paweł Głowacki, Krzysztof Kawalec, Adam Kozakiewicz, Jerzy Szczeciński. 2009. *Lotnicze zespoły napędowe.* Część 1. Warszawa: Wydawnictwo WAT.

[12] Urasiński Piotr. 2001. „Oddymianie i optymalna zabudowa wentylatorów osiowych". *Polski Instalator* 2.

[13] Xuemin Ye, Li Pengmin, Li Chunxi, Ding Xueliang. 2015. "Numerical investigation of blade tip grooving effect on performance and dynamics of an axial flow fan". *Energy* 82 : 556 - 569.

[14] Yang Li, Ouyang Hua, Du Zhao-Hui. 2007. "Optimization design and experimental study of low-pressure axial fan with forward-skewed blades". *International Journal of Rotating Machinery* (10 pages).

[15] Novovent, Winder, http://www.novovent.com/assets/files/pdf/descargas/eng/Winder-erp2015-2013-12pag-Novovent.pdf.

[16] Zitron, Fan Protection, http://www.zitron.com/download/FanProtection.pdf.

Analiza wytrzymałościowa łopaty osiowego wentylatora kanałowego

Marek ROŚKOWICZ, Ryszard CHACHURSKI, Sławomir TKACZUK, Piotr LESZCZYŃSKI, Maciej MAJCHER, Łukasz OMEN

Wojskowa Akademia Techniczna, Wydział Mechatroniki i Lotnictwa, ul. gen. Witolda Urbanowicza 2, 00-908 Warszawa

Streszczenie. W pracy przedstawiono numeryczną analizę wytrzymałościową łopaty osiowego wentylatora kanałowego. Wentylatory tego typu stanowią liczną grupę maszyn przepływowych. Wykonana analiza miała na celu określenie przyczyn powtarzających się cyklicznie awarii zespołu wentylacyjnego. Zaprezentowano sposób odwzorowania geometrii łopaty wentylatora poprzez zastosowanie metody inżynierii odwrotnej. Przy odwzorowywaniu geometrii wykorzystano skany otrzymane za pomocą skanera optycznego na zasadzie triangulacji. Następnie przedstawiono założenia upraszczające, na których oparte zostały obliczenia numeryczne. Obliczenia te przeprowadzono dla eksploatacyjnych prędkości obrotowych wirnika wentylatora. Z kolei opisano przebieg samych obliczeń numerycznych, a także przedstawiono uzyskane wyniki. Wyniki te zaprezentowano w postaci kolorowych map rozkładu naprężeń dla wybranych elementów konstrukcji łopaty. Rozkład naprężeń w przekroju poprzecznym łopaty porównano z tomograficznymi fotografiami przełomów zniszczonych piór łopat wirnika. Opracowano wnioski końcowe, z których wynika, że w procesie konstruowania wentylatorów powinna być wykonana optymalizacja nie tylko w obszarze jego sprawności, ale również w obszarze parametrów wytrzymałościowych i użytkowych, w tym między innymi trwałości eksploatacyjnej urządzenia.

Słowa kluczowe: wentylator osiowy, inżynieria odwrotna, obliczenia numeryczne, obliczenia wytrzymałościowe